A Hybrid Approach for Brain Tissue Segmentation: Integrating Gaussian Mixture Models with Atlas-based and Tissue Modeling Techniques

X. Beltran Urbano[1] and F. Hartmann[1]

[1] *University of Girona, Erasmus Mundus Joint Master Degree in Medical Imaging and Applications (MAIA)*

Abstract—Brain tissue segmentation is crucial in medical imaging for accurately distinguishing different brain areas and is essential for diagnosing and treating neurological conditions. It also significantly aids neuroscientific research by allowing for in-depth study of brain structure and function, advancing our knowledge of the brain. In this report, two of the most popular techniques are combined: the Gaussian Mixture Model and the Probabilistic Atlas. For this, multiple initialization types, independent segmentation tasks, and different atlases are compared. It has been shown that using a Gaussian mixture model and an atlas built from images from the same scanner and a similar patient demographic improves segmentation performance but might result in lower generalizability.

Keywords—Brain tissue segmentation, Probabilistic Brain Atlas, Tissue Probability Models, Expectation Maximisation (EM), Gaussian Mixture Models (GMM), Magnetic Resonance Imaging (MRI)

I. INTRODUCTION

In the discipline of medical imaging, image segmentation is among the oldest techniques utilized. In order to enhance patient diagnosis and treatment, the objective of this procedure is to segment the image into subregions. A conventional method in brain imaging is to divide an image of the brain into a collection of distinct regions that share similar characteristics (such as intensity, texture, homogeneity, and so forth) in order to extract the tissue. The methodology of tissue segmentation from magnetic resonance (MR) images, including grey matter (GM), white matter (WM), and cerebrospinal fluid (CSF), is commonly employed in the domain of quantitative brain analysis. Diseases such as Alzheimer's disease (AD), Parkinson's disease, and others can be better identified and, hence, treated.

This segmentation can be accomplished using either unsupervised or supervised algorithms. Clustering is among the most frequently employed algorithms for this aim. In this laboratory, the primary objective is to implement different segmentation approaches, including clustering methods, probabilistic atlases, and intensity information maps.

II. DATASET

The dataset utilised to perform this laboratory contains 20 cases. For each case, a T1-weighted scan and a ground truth (GT) consisting of segmentation masks corresponding to white matter (WM), grey matter (GM), and cerebrospinal fluid (CSF) are provided. An example of the different image modalities of the dataset can be observed in Figure 1.

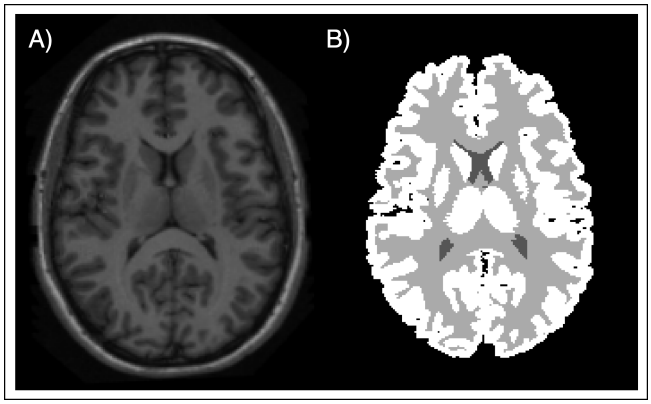

Fig. 1: An example of the different modalities of the dataset **A)** T1-weighted **B)** GT

III. METHOD

I. Atlas registration

Prior to the segmentation, a registration step was performed to register the atlas, i.e., the mean image, to the target. For this step, a rigid, an affine, and a multi-resolution b-spline registration were carried out in this order. To accomplish a multi-resolution registration, a six-level pyramid was chosen. Furthermore, an advanced normalised correlation metric with a transform bending energy penalty is chosen as proposed by [2]. All parameter files are available on modelZoo. All registrations were computed using itk-elastix [1].

II. Segmentation without GMM

1. Segmentation using Tissue Models

Among the various segmentation methods tested in this experiment, tissue model segmentation was the primary choice. This approach relies solely on voxel intensity data for segmentation, thereby excluding spatial information from the images. Previously, we computed a 256×3 matrix (the Tissue Models Probabilities), where *256* represents the probability of the normalised intensity values of the images, and 3 corresponds to the brain's tissue types. For segmentation, values 1, 2, and 3 were assigned to WM, GM, and CSF, respectively, for each intensity level in the range $[0, 255]$, based on the highest probability across the three tissue types. The formula used is as follows:

$$\text{TissueModel} = \underset{j \in \{0,1,2\}}{\text{argmax}} \ (\text{Prob}[i, j]) \quad \text{for } i = 0, 1, \ldots, 255 \tag{1}$$

After computing the highest probability across the three tissue types, we have used this information to change each pixel intensity value of the original image by the corresponding value of the tissue model. As a result of this, an image segmented into WM, GM, and CSF is obtained.

2. Segmentation using propabalistic atlas

For this segmentation, unlike the previous segmentation approach, the only information used to segment the image is the spatial information of the pixels. Before segmenting the image, as explained in the subsection I, we registered the probabilistic atlas, which was computed in the previous lab, to each of the images in the dataset. Then, similarly to the previous step, values 1, 2, and 3 were assigned to WM, GM, and CSF, respectively, for each pixel of the image, based on the highest probability across the three tissue types. The formula used is as follows:

$$\text{Segmentation} = \underset{l \in \{1,2,3\}}{\text{argmax}} \ (\text{Prob}[i, j, k, t]) \quad \text{for each } (i, j, k) \tag{2}$$

where:

- i, j, k are the indices representing the spatial dimensions (x, y, z) of the image.
- t is the index representing the different tissue types in the fourth dimension of the Probabilistic Atlas.

After computing this formula, the image tissue segmentation is acquired.

3. Segmentation using Both Approaches

After computing the previous segmentations, in which we used intensity information and spatial information independently, we have computed a final approach consisting of a combination of both of them. To perform this combination, we have utilised the tissue models to create an image of intensity probabilities. Subsequently, we have multiplied the intensity probability image by the probabilistic atlas. As a result, a 4D image with the probabilities of each of the tissues, is created. Then, as a last step, following the same methodology, values 1, 2, and 3 were assigned to WM, GM, and CSF, respectively, for each pixel of the image, based on the highest probability across the three tissue types. The formula explaining this entire process is as follows:

· Compute segmentation for each tissue:

$$\text{intensityProb}_t = \sum_{i=0}^{255} \text{tissueModels}_{i,t} \cdot \mathbb{I}_{\text{image}=i} \tag{3}$$

· Multiply by Probabilistic Atlas:

$$\text{probImage}_t = \text{intensityProb}_t \cdot \text{atlasProb}_t \tag{4}$$

· Finally, determine the segmentation:

$$\text{finalSeg}_{x,y,z} = \underset{t \in \{1,2,3\}}{\text{argmax}} \ (\text{probImage}[x, y, z, t]) \tag{5}$$

where:

- $\text{tissueModels}_{i,t}$ represents the probability value for intensity level i and tissue type t.
- $\mathbb{I}_{\text{image}=i}$ is an indicator function that is 1 where the image intensity is i and 0 elsewhere.
- atlasProb_t is the probabilistic atlas for tissue t.
- $\text{finalSeg}_{x,y,z}$ is the final segmentation label for voxel (x, y, z).

III. Segmentation with GMM

1. Improvements in GMM computation

In comparison to the last implementation of the Gaussian Mixture Model, multiple changes have been made. Firstly, redundant calculations have been removed. Secondly, the convergence criteria have been adapted to allow for faster convergence with similar robustness. The new convergence criteria can be seen in Equation 6:

$$|\log(\phi_{t+1}) - \log(\phi_t)| < \varepsilon \tag{6}$$

where

$$\phi = \frac{1}{N} \sum_{i=1}^{N} p_i(\underline{x}|\theta) \tag{7}$$

with

$p(\underline{x}|\theta)$: Probability density function
θ : Parameters of the model
N : Number of Pixels

In this formula, the value ε was chosen empirically as 10^{-6}. Additionally, if no convergence is reached after 500 iterations the algorithm is stopped. Thirdly, and most importantly, the computation of the probability density function has been changed. More specifically, the computation of the Mahalanobis distance has been adapted after [3] using the Cholesky decomposition, allowing for faster computation.

The Cholesky decomposition of the covariance Σ is given by Equation 8.

$$\Sigma = LL^T \tag{8}$$

The computation of the Mahalanobis distance can be changed to Equation 9

$$\underline{x}\,\Sigma^{-1}\,\underline{x}^T = \underline{x}\,(LL^T)\,\underline{x}^T = (L^{-1}\underline{x})^2 \tag{9}$$

where

$\underline{x}$: data

L : Lower triangular Cholesky decomposition

2. Initialization Methods

Four different initialization methods are available.

- K-means
- Tissue Model
- Probabilistic Atlas
- Probabilistic Atlas and Tissue Model

While the first two are used to initialise the means, the probabilistic atlas is used to initialise the membership weights. This allows the computation of one maximisation step in-between, resulting in updated covariance, means, mixture weights, and membership weights. In the last method, the means of the tissue model and the covariance, mixture, and membership weights of the atlas are used.

3. Integration of the Probabilistic atlas

THe atlas integration into the segmentation process can occur at various stages: prior to, during, or after the Gaussian Mixture Model computation. When added afterwards, it involves multiplying the atlas probabilities with the membership weights. When used during the computation, the atlas probabilities are multiplied by the membership weights in every iteration; after the expectation step.

IV. Results

I. Metrics

To evaluate the effectiveness of our approach and analyse the laboratory experiments, we assessed the various cases in our dataset using two key metrics: the Dice Score (DSC), as outlined in Equation 10, and the *Balanced Accuracy (BA)*, which is presented in Equation 11.

$$DSC = \frac{2 \times TP}{2 \times TP + FP + FN} \tag{10}$$

$$\text{Balanced Accuracy} = \frac{\text{Specificity} + \text{Sensitivity}}{2} \tag{11}$$

Both the mean and standard deviation were calculated during the tests in order to enhance the available information and afterwards analyse the data in a comprehensive manner.

II. Experiments

In this section, the results of the experiments performed are shown. The results will be split into multiple parts. First, the segmentation without a Gaussian mixture model. Second, the segmentation using GMM and the initialization types previously mentioned. Third, the segmentation using the atlas before and during the computation of the Gaussian Mixture Model

1. Quantitative results

As previously stated, the dice score and balanced accuracy have been used to evaluate this project. This evaluation can be observed in Table 1 and Table 2 for the experiments explained in subsection II, and subsection III, respectively. In addition, an evaluation of the best approaches, the use of the probabilistic atlas before and after the GMM, and the segmentation by utilising the MNI atlas, can be observed in Table 3.

2. Quantitative results

In order to provide a more accurate evaluation of the different approaches implemented in this project, qualitative results are provided. In Figure 4, we can observe an example of the segmentation of case 1109 for all the different strategies carried out in this project. In addition, in Figure 5, we can observe the results obtained by utilising the MNI atlas to accomplish this segmentation task.

V. Discussion

In this section, the different results of this project will be discussed and compared to each other.

I. Comparison of different segmentation approaches

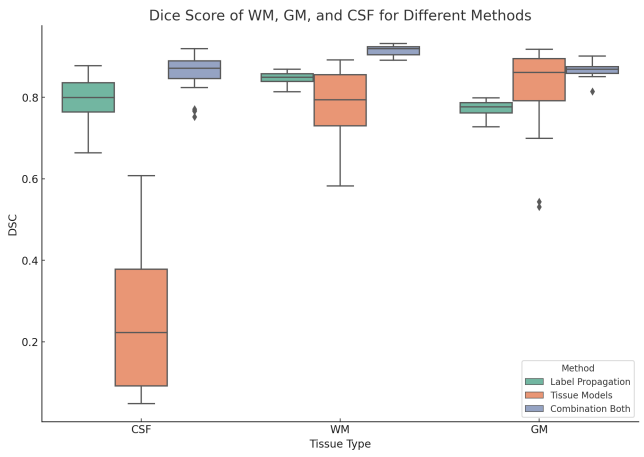

Fig. 2: Comparison of the dice obtained for each of the approaches and tissues.

As explained in subsection II, brain tissue segmentation can be implemented by using intensity information (tissue models), spatial information (propabalistic atlas), or a combination of both. Table 1 shows the resulting dice scores of testing our dataset with different approaches, which are explained in Section III. The results demonstrated good performance using the different approaches, leading to similar re-

TABLE 1: RESULTS OF DIFFERENT SEGMENTATION APPROACHES WITHOUT USING GMM ALGORITHM

Initialization	**Dice: mean ± std**			**BA**	**Time [s]**
	CSF	*WM*	*GM*		
Tissue Models	0.247 ± 0.164	0.780 ± 0.087	0.816 ± 0.111	0.614 ± 0.100	**0.644 ± 0.101**
Propabalistic Atlas	0.790 ± 0.055	0.846 ± 0.015	0.771 ± 0.019	0.802 ± 0.025	1.478 ± 0.531
Combination of Both	**0.856 ± 0.050**	**0.915 ± 0.012**	**0.867 ± 0.018**	**0.879 ± 0.021**	108.320± 19.230

TABLE 2: RESULTS OF DIFFERENT INITIALIZATION TYPES

Initialization	**Dice: mean ± std**			**BA**	**Time [s]**
	CSF	*WM*	*GM*		
K-means	0.196 ± 0.289	**0.879 ± 0.089**	0.792 ± 0.053	0.703 ± 0.106	40.163 ± 21.664
Tissue Model	0.300 ± 0.313	0.854 ± 0.096	0.839 ± 0.049	**0.746 ± 0.087**	**18.277 ± 14.510**
Propabalistic Atlas	**0.307 ± 0.319**	0.831 ± 0.108	**0.840 ± 0.044**	0.737 ± 0.082	21.220 ± 11.963

TABLE 3: RESULTS OF DIFFERENT INITIALIZATIONS AND ATLAS INTEGRATION POINTS

Initialization	**Atlas Integration**	**Dice: mean ± std**			**BA**	**Time [s]**
		CSF	*WM*	*GM*		
Best initialization*	After	**0.729 ± 0.092**	0.935 ± 0.013	0.883 ± 0.026	**0.870 ± 0.047**	16.5 ± 14.2
	Into	0.623 ± 0.139	**0.948 ± 0.010**	**0.920 ± 0.014**	0.830 ± 0.044	29.9 ± 23.0
Tissue Model & Propabalistic Atlas	After	0.354 ± 0.282	0.850 ± 0.108	0.848 ± 0.049	0.756 ± 0.068	21.4 ± 18.1
	Into	0.337 ± 0.252	0.876 ± 0.066	0.661 ± 0.332	0.625 ± 0.123	**11.5 ± 6.0**
MNI Atlas & Best Initialization*	Into	0.374 ± 0.152	0.884 ± 0.017	0.792 ± 0.040	0.756 ± 0.068	29.9 ± 23.0

**Best initialization refers to the "Tissue Model" method in this context.*

sults. However, in the case of the tissue models, for the CSF tissue, we can observe an abrupt gap between the dice obtained by the tissue model approach and the dice obtained by the other methods. This can be explained by the fact that the ground truth has been wrongly annotated, since some parts of the CSF close to the skull are missing. As a result, when segmenting these regions with the tissue models, the dice decrease considerably since it is interpreted as the wrong tissue. On the contrary, with the other approaches, we are using the probabilistic atlas and, hence, providing spatial information to the segmentation. Since this atlas has been built using the GT that has been wrongly annotated, the obtained segmentations have a higher dice score due to the fact that the missing part of the CSF is missing in the atlas too.

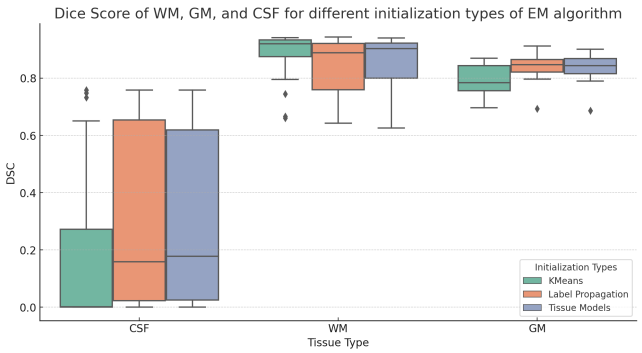

Fig. 3: Comparison of the dice obtained for each of the initialization types of EM algorithm

II. Comparison of GMM initialization

The Gaussian Mixture Model was initialised with three different initialization types as specified in: K-means, tissue model, and propabalistic atlas. For all initialization types, the segmentation of white matter and grey matter is good, with dice scores ranging from 0.77 to 0.87. The detailed results are visible in Table 2. However, the segmentation of the cerebrospinal fluid is performing significantly worse, with dice scores ranging from 0.19 to 0.30. Similarly than in the previous section, this can be attributed partly to the missing annotation of the cerebrospinal fluid close to the skull, as displayed in Figure 4. Furthermore, it can be noted that K-means initialization achieves slightly worse results in terms of balanced accuracy than tissue model and propabalistic atlas initialization: 0.70 vs. 0.73 and 0.74, respectively. This difference could have resulted from a-priori information about the dataset in the form of the training set (n = 15) used to build the atlas and the tissue model. Due to the fact that the training and test sets were recorded on the same scanner, knowledge about the intensity distributions was similar and therefore provided meaningful information. Finally, it can be noted that the initialization with the means of the tissue model led to the most stable results in terms of balanced accuracy. This is especially interesting as the tissue model was not the top-performing segmentation initialization in terms of dice score for any of the tissues.

III. Comparison of Atlas Integration Points

Based on the results from the last section, the best initialization was chosen to be the means of the tissue models. The probabilistic atlas can be added after GMM or during. The quantitative results can be seen in Table 3. The quality of the segmentations with respect to the dice score and the balanced accuracy are significantly better when the Gaussian mixture model is initialised with the tissue model. This is most apparent in the dice score of the cerebrospinal fluid: 0.35 with the tissue model and atlas versus 0.72 when only using the tissue model. Furthermore, comparing the balanced accuracy when integrating the atlas after or into the GMM, a relative big difference is observed: 0.62 vs. 0.75 (Tissue Model and Probabilistic Atlas Initialization) and 0.83 vs. 0.87, respectively (Tissue Model Initialization). One might be tempted to say that applying the atlas after the EM leads to significantly better results. However, upon comparing the qualitative results, observing Figure 4, image I) and J), the integration of the atlas into the EM showed a smoother segmentation, especially of the cerebrospinal fluid. This remained true upon visual inspection of the other cases and slices.

IV. Comparison with MNI Atlas

To allow for comparison with the MNI Atlas, the best initialization and integration of the EM have been chosen as tissue model initialization and integration into the GMM. This decision has been made taking both quantitative and qualitative results into account. Comparing the qualitative results of the best previous approach, compared to the same approach using the MNI atlas in Figure 5, shows a significantly worse segmentation of the cerebrospinal fluid. This observation is confirmed quantitatively in Table 3 with a Dice Score of 0.37. It is worth mentioning that the segmentation of white and grey matter is solid, with dice scores of 0.88 and 0.79. The difference in quality can be partly attributed to the fact that the MNI atlas has been built using images from a different demographic and from a different scanner, resulting in different intensity distributions. As mentioned before, the low results of the CSF can also be attributed to the imperfections in the ground truth. Nevertheless, the segmentation using the MNI atlas shows significant errors at the lateral ventricles too.

VI. Conclusion

To conclude, it is evident that an atlas created from similar data shows superior segmentation results. On the other hand, a common space such as MNI is often required to accurately compare between datasets. Additionally, the effectiveness of the tissue model has been shown, as its adaptation resulted in top-performing results among all tested approaches. In comparison to a standalone Gaussian Mixture Model, the integration of both probabilistic atlas and tissue models improved dice scores significantly. Even as a standalone approach and especially in combination with the probabalistic atlas, the tissue model showed excellent performance. In the future, we hope to integrate the method or the ideas learned into a deep learning framework. Hence, we are very enthusiastic to work on the upcoming multi-atlas and deep-learning-based brain tissue segmentation.

VII. Design and implementation

When creating our hybrid approach for brain tissue segmentation, we strictly followed object-oriented programming principles, building our solution from the ground up in a modular fashion. The implementation was firmly based on the theoretical concepts covered in our theory lectures, providing a solid academic foundation. This systematic approach allowed us to gain a thorough understanding of the algorithm's components as we carefully assembled each function in the class.

VIII. Project Management

This project, collaboratively undertaken by two team members, was initiated from the ground up, requiring creative thinking and comprehensive planning. Contrary to initial expectations, the project was completed faster than anticipated, thanks to the robust code base established in previous projects. Building upon the foundation of the previous projects to enhance performance further, we were excited to see the advancements and improvements our efforts had and hopefully will yield.

References

[1] Stefan Klein et al. "elastix: A Toolbox for Intensity-Based Medical Image Registration". In: *IEEE Transactions on Medical Imaging* 29.1 (2010), pp. 196–205. DOI: 10.1109/TMI.2009.2035616.

[2] Inge A. Mulder et al. "Automated Ischemic Lesion Segmentation in MRI Mouse Brain Data after Transient Middle Cerebral Artery Occlusion". In: *Frontiers in Neuroinformatics* 11 (2017). ISSN: 1662-5196. DOI: 10.3389/fninf.2017.00003. URL: https://www.frontiersin.org/articles/10.3389/fninf.2017.00003.

[3] Zen. *Efficient/Fast Mahalanobis Distance Computation*. Stack Exchange: Cross Validated. 2020. URL: https://stats.stackexchange.com/q/147222 (visited on 11/20/2023).

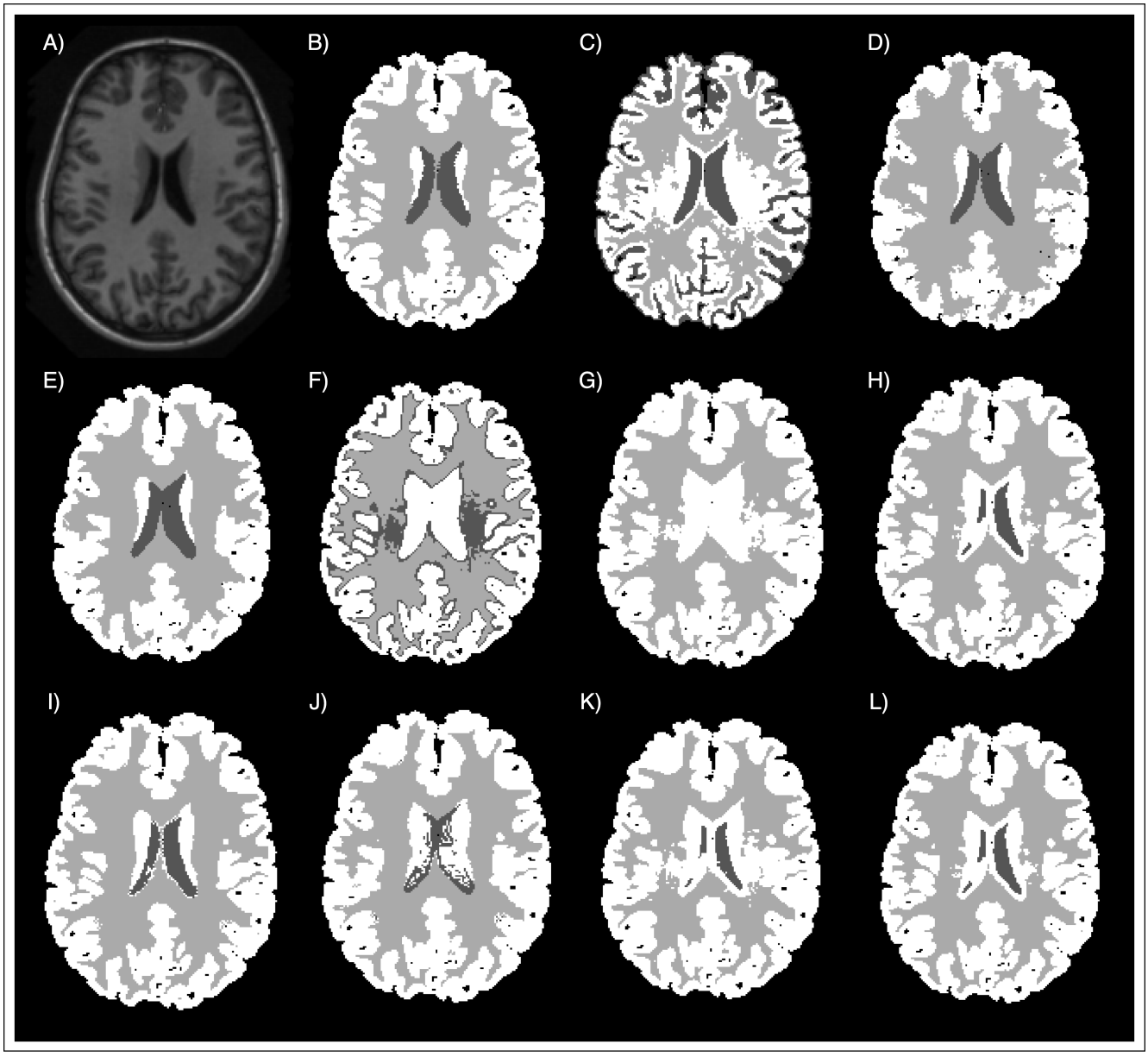

Fig. 4: Example of the different results obtained in this project. **A)** Original Image **B)** GT **C)** Tissue Models Segmentation **D)** Probabilistic Atlas Segmentation **E)** Combination of C and D **F)** KMeans Initialization for GMM **G)** Tissue Models Initialization for GMM **H)** Probabilistic Atlas Initialization for GMM **I)** Best Approach (Tissue Models) including Probabilistic Atlas Into GMM algorithm **J)** Best Approach (Tissue Models) including Probabilistic Atlas After EM algorithm **K)** Tissue Model & Propabalistic Atlas Initialization For GMM including Probabilistic Atlas After GMM algorithm **L)** Tissue Model & Propabalistic Atlas Initialization for GMM including Probabilistic Atlas Into GMM algorithm

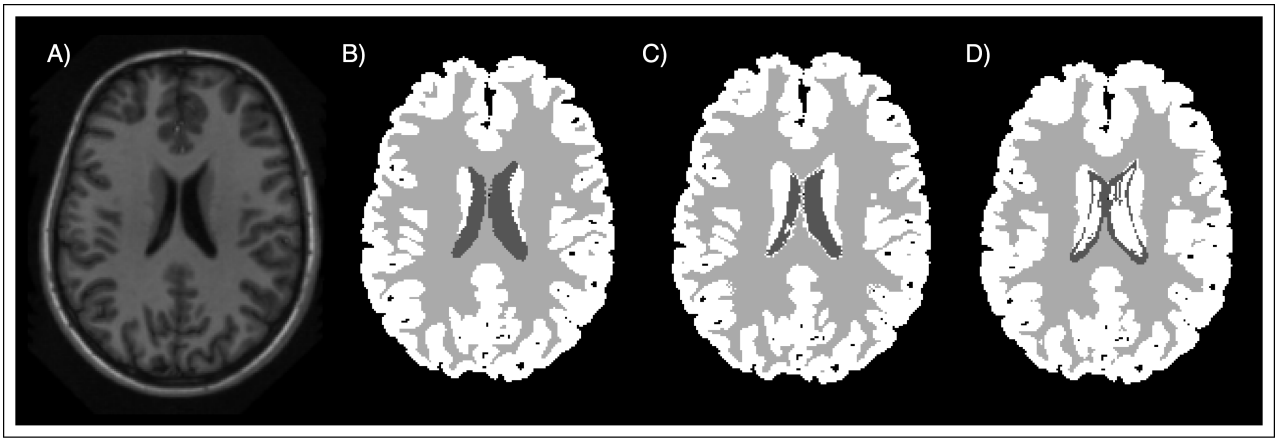

Fig. 5: Example of the segmentation by employing the MNI atlas. **A)** Original Image, **B)** Ground Truth, **C)** Best segmentation by employing our atlas, **D)** MNI segmentation